Enhancing wound dressing efficiency: Cellulose nanofiber sponges loaded with Ganoderma lucidum mycelium fractions

Citation for the original published paper (version of record):
Rincón, E., Nejati, M., Zha, L. et al (2026). Enhancing wound dressing efficiency: Cellulose nanofiber sponges loaded with Ganoderma lucidum
mycelium fractions. International Journal of Biological Macromolecules, 337.
http://dx.doi.org/10.1016/j.ijbiomac.2025.149401

International Journal of Biological Macromolecules 337 (2026) 149401

Contents lists available at ScienceDirect

International Journal of Biological Macromolecules

journal homepage: www.elsevier.com/locate/ijbiomac

Enhancing wound dressing efficiency: Cellulose nanofiber sponges loaded with Ganoderma lucidum mycelium fractions

Esther Rincón [a], Maryam Nejati [b], Li Zha [c,d], Eduardo Espinosa [a], Amparo Jiménez-Quero [c,d,*]

[a] BioPrEn Group (RNM940), Chemical Engineering Department, Instituto Químico para la Energía y el Medioambiente (IQUEMA), Faculty of Science, Universidad de Córdoba, 14014, Córdoba, Spain
[b] Department of Molecular Biosciences, The Wenner-Gren Institute, SciLifeLab, Stockholm University, SE-106 91, Sweden
[c] Division of Industrial Biotechnology, Department of LIFE Sciences, Chalmers University of Technology, 412 96, Gothenburg, Sweden
[d] Wallenberg Wood Science Center, Department of LIFE Sciences, Chalmers University of Technology, 41296, Gothenburg, Sweden

ARTICLE INFO

Keywords:
Cellulose nanofibers (CNF)
Ganoderma lucidum
Wound dressing
Mycelium-based biomaterials
Exopolysaccharides (EPS)
Porous sponges

ABSTRACT

In this study, cellulose nanofiber (CNF)-based sponges incorporating different *Ganoderma lucidum* biomass fractions were developed and evaluated as bioactive wound dressing materials. Isolated mycelium (G-M), mycelium with exopolysaccharide (G-ME) and purified exopolysaccharide (G-E) fractions were characterized to determine their composition and functionality. The incorporation of fungal biomass significantly altered the structural and physical properties of CNF-based sponges, leading to reduced bulk density, high porosity (>99 %) and increased specific surface area (up to 7.4 m^2/g). The type of fungal fraction influenced material behavior: G-M enhanced water absorption (up to 9200 %) and compressive strength, G-E improved network stability and reduced degradation rate in PBS, and G-ME produced the most homogeneous pore structure and highest tensile strength (30 MPa). Scanning electron microscopy (SEM) confirmed a highly interconnected porous morphology with an average pore size close to 100 μm, comparable to those reported for skin substitutes. The sponges exhibited excellent swelling capacity, controlled degradation, and rapid exudate uptake (up to 400 %), confirming their suitability for wound exudate management. Biological evaluations demonstrated hemocompatibility, high cytocompatibility (>90 % cell viability in HaCaT cells), and antioxidant activity. Notably, sponges containing EPS-rich fractions (CNF:G-E and CNF:G-ME) showed a clear bactericidal effect against *Staphylococcus aureus*, a major wound pathogen, while maintaining superior mechanical and fluid absorption performance. Overall, these findings demonstrate that fungal biomass can act as a natural, low-cost additive to tailor the structure, stability, and bioactivity of CNF-based dressings without extensive purification. The combination of mechanical resilience, biocompatibility, and selective antimicrobial activity supports their potential as multifunctional and sustainable wound dressing materials.

1. Introduction

Biomaterials are increasingly used in biomedical and tissue engineering applications [1]. Among these, polymer-based biomaterials have attracted particular attention due to their versatility, high water retention, and porous structures [2]. Within this category, biopolymers stand out for their biocompatibility and sustainable origin, making them suitable for medical applications such as wound dressings and regenerative scaffolds [3].

Wound healing is a complex process involving hemostasis, inflammation, proliferation, and remodeling. Effective control of wound exudate is critical, as excess fluid can lead to hyperhydration, tissue damage, and delayed healing. Conventional dressings often do not provide adequate control, which has driven the development of advanced porous materials such as aerogels, foams, and sponges [4]. Cellulose nanofibers (CNFs) have emerged as promising candidates for such applications. Their abundance of hydroxyl groups gives them chemical versatility, while their high crystallinity, water dispersibility, and three-dimensional network structure provide mechanical stability and excellent fluid absorption [3]. CNFs have been successfully used in gel- and sponge-shaped wound dressings, demonstrating hemostatic and bioactive agent delivery functions [5,6]. Recent studies also highlight their potential as functional dressings with customized mechanical and biological performance [7–10].

* Corresponding author at: Division of Industrial Biotechnology, Department of LIFE Sciences, Chalmers University of Technology, 412 96, Gothenburg, Sweden.
E-mail address: amparo@chalmers.se (A. Jiménez-Quero).

https://doi.org/10.1016/j.ijbiomac.2025.149401
Received 21 July 2025; Received in revised form 26 November 2025; Accepted 30 November 2025
Available online 5 December 2025

Along with cellulose, microbial exopolysaccharides offer unique bioactivity. Among them, fungal exopolysaccharides (EPS) show immunomodulatory, antioxidant, and wound-healing potential [11,12]. *Ganoderma lucidum*, a well-known medicinal mushroom, produces polysaccharides with diverse structural characteristics and biological effects [13,14]. However, most studies have focused on extracts from spores or fruiting bodies, which require long cultivation periods and produce limited quantities. Mycelium-derived fractions, including associated EPS, represent a faster and more sustainable alternative, but their potential in wound healing applications remains under-explored [15].

Despite the recognized advantages of CNFs and *G. lucidum* polysaccharides separately, their combination in porous, highly absorbent sponges for wound healing has not been reported. This study addresses this gap by developing CNF-based sponges enriched with *G. lucidum* mycelium fractions. The influence of the isolated mycelium, mycelium with EPS, and pure EPS fractions on the chemical, structural, morphological and mechanical properties of the sponges has been investigated. In addition, their liquid management behavior and biological performance were evaluated to determine their suitability as advanced materials for wound treatment.

2. Materials and methods

2.1. Materials

CNFs were prepared from wheat straw bleached cellulose pulp by high-pressure homogenization after a chemical pretreatment consisting of a TEMPO-mediated oxidation reaction as explained in previous investigations [16].

All media components used in the cytotoxicity assay were purchased from Gibco, Thermo Fisher Scientific, USA and MTT (3-(4, 5-dimethylthiazolyl-2)-2, 5-diphenyltetrazolium bromide) was purchased from Invitrogen, Thermo Fisher Scientific, USA. All chemicals were purchased from Sigma-Aldrich (Stockholm, Sweden), if not specified otherwise.

2.2. Preparation and characterization of fungal biomass

2.2.1. Production of fungal biomass

The fungal biomass (FB) was produced by culturing *Ganoderma lucidum* (strain M9725, Mycelia, Belgium) on potato dextrose broth (PDB). The cultures were incubated at 30 °C for 12 days. The resulting biomass was then washed with Milli-Q water and the exopolysaccharide was separated from the mycelium by gentle scraping, obtaining the three fractions of FB: *G. lucidum* mycelia + exopolysaccharide (G-ME), *G. lucidum* mycelia (G-M), and *G. lucidum* exopolysaccharide (G-E). The biomasses were then frozen in liquid nitrogen and freeze-dried (Labconco FreeZone 6, with bulk tray drier, USA).

2.2.2. Characterization of fungal biomasses

2.2.2.1. Carbohydrate composition. The monosaccharide composition of the FB was analyzed via both sulfuric acid and trifluoroacetic acid (TFA) hydrolysis. To perform the sulfuric acid hydrolysis, 4 mg of samples were weighed in glass tubes and 125 μL of 72 % sulfuric acid was added to the tubes, followed by incubation for 1 h at room temperature. Subsequently, 1375 μL of Milli-Q water was added to the samples and hydrolyzed for another 3 h at 100 °C. The resulting solution was filtered (0.2 μm, Chromacol nylon filters, Thermo Scientific, USA) and diluted in Milli-Q water for analysis in HPAEC-PAD (high-performance anion-exchange chromatography/pulsed amperometric detection, Dionex 6000, Thermo Scientific, USA) through Dionex CarboPac PA20 column. The eluent started as water plus 1.2 % of 200 mM sodium hydroxide, which after 18 min was changed to 100 % 200 mM NaOH and maintained for 20 min. Finally, during the last 5 min the composition was returned to 1.2 % of 200 mM NaOH in water. The flow rate was constant at 0.4 mL/min. For the TFA test, 2 mg of dry powdered FB was weighed in glass tubes to which 1 mL of 2 M TFA was added. The tubes were then incubated at 120 °C for 3 h. After filtration, 100 μL of the solution was dried under air flow, reconstituted in Milli-Q water, and analyzed by HPAEC-PAD in the same manner as sulfuric acid lysate samples. The analysis was performed in triplicate for each type of sample, and the results were expressed as the arithmetic mean ± standard deviation.

2.2.3. Phenolic acids determination

To investigate the phenolic acid composition of the FB, 0.5 mL of 2 M NaOH was added to triplicate samples of 10 mg of FB. The Eppendorf tubes were then flushed with N_2 and incubated overnight at 60 °C under stirring. The mixtures were then acidified to pH 3 using 12 M HCl, and the phenolic compounds were extracted by liquid-liquid partitioning with ethyl acetate (4×) [17]. The organic phase was dried and reconstituted in methanol, and the total phenolic content was determined using the Folin-Ciacalteu method [18]. In addition, an aliquot of the methanolic extracts was analyzed through ZORBAX StableBond C18 column (Agilent Technologies, Santa Clara, CA, USA) in HPLC/UV–Vis (Agilent 1200 Series, Agilent Technologies, USA) as described in a previous work [19]. Various concentrations (100–5 μg/mL) of gallic, caffeic, sinapic, cinnamic, ferulic and p-coumaric acids were used as external standards. The analysis was performed in triplicate for each type of sample, and the results were expressed as the arithmetic mean ± standard deviation.

2.2.4. Protein content

Soluble protein content of the FB was measured by Bradford assay (Bio-Rad Protein assay kit, USA) [20]. The test was done according to the kit instructions for microplate format. Bovine serum albumin was used as the standard and the soluble protein content was calculated as a percentage of the initial biomass. The analysis was performed in triplicate for each type of sample, and the results were expressed as the arithmetic mean ± standard deviation.

2.2.5. Fourier transform infrared spectroscopy (FTIR)

FTIR analyses of FB were performed using a spectrometer FTIR-ATR Perkin Elmer Spectrum Two, in the range of 4000–400 cm^{-1} with a resolution of 4 cm^{-1} and a total of 40 scans averaged per spectrum.

2.2.6. Zeta potential

The zeta potential of FB was measured using a Zetasizer (ZSP, Malvern Instrument Ltd., Worcestershire, UK) at 25 °C based on laser Doppler velocimetry. Dispersions were prepared at a concentration of 10^{-3} g/mL using distilled water as solvent and inert electrolyte. The refractive index values for dispersant and the material (β-glucans) were set as 1.33 and 0.146, respectively. The analysis was performed in triplicate for each type of sample, and the results were expressed as the arithmetic mean ± standard deviation.

2.3. Bio-based sponges' production

Prior to sponge formation, hydrogel suspensions were prepared. In all cases, they were formulated so that the final weight of each sponge was 0.075 g (dry matter) with a 6 cm-diameter. Four types of hydrogels were produced: a control (100 % CNF), and three 90:10 CNF: FB formulations (each containing one of the three FB fractions). First, the corresponding amount of FB was weighed, and the required volume of CNF suspension was added. The mixtures were brought to a total of 15 g with distilled water. This mixture was homogenized in a high-shear homogenizer (IKA T18 digital Ultra Turrax) for 3 min at 10,000 rpm and then left under magnetic stirring for 24 h to allow the physical cross-linking between the polymers to occur. After this, the solution was poured into Petri dishes (Ø 6 cm) and freeze-dried at −80 °C for 72 h under a vacuum of 0.5 mBar.

2.4. Sponges' characterization

2.4.1. Physical properties

The bulk density of the prepared sponges was determined from the dimensions (height, diameter, and thickness) and the weights of the samples. The porosity of the sponges was estimated using Eq. (1), proposed by Geng (2018) [21].

$$\text{Porosity}\ (\%) = (V - W/\rho)/V \times 100 \quad (1)$$

where V is the volume (cm^3) of the sponges, W is the weight (g) of the sponges, and ρ is the density of the cellulose (1.528 g/cm^3). Bulk density and porosity were determined for four replicates of each sponge, and the results were expressed as the arithmetic mean ± standard deviation.

Nitrogen physisorption analysis was performed using a Micromeritics Tristar 3000 instrument (Micromeritics Instrument Corp., USA) at 77 K with nitrogen (N_2) as the adsorption gas. Prior to measurement, the samples were degassed for 24 h at 50 °C under vacuum to remove residual moisture. The adsorption-desorption isotherms were recorded, and the Brunauer–Emmett–Teller (BET) method was applied to determine the specific surface area using MicroActive software from Micromeritics.

X-Ray diffraction (XRD) analyses were performed using a Bruker D8 Discover with a CuKα1 source over an angular range of 10–80° at a scan speed of 0.025°/s in reflection mode. Fourier Transform Infrared spectroscopy (FTIR) analyses were performed as previously described.

Scanning Electron Microscopy (SEM) images were captured using a Hitachi TM-1000 tabletop microscope (Japan), operated at a voltage of 10 kV and a working distance of 6 mm. SEM samples were prepared by cryo-fracturing with the aid of liquid nitrogen. These samples were subsequently affixed onto a metal support and securely positioned using copper tape. The pore diameters in each sponge were quantified using ImageJ software (US National Institutes of Health, USA) and were determined as the mean value from a minimum of 80 random measurements. The pore size distribution histograms and average pore size (APS) of the sponges were analyzed by fitting the data using a Gauss curve fitting procedure.

The water absorption capacity of the sponges was measured gravimetrically as follows. Briefly, a square piece of 4 cm^2 of each sponge sample was weighed (W_0) and immersed in 10 mL of distilled water. The samples were taken out after 20 min and left to stand on a Petri dish for 1 min before weighing the sample again (W_f). Then, the water absorption capacity of the sponges was calculated according to the Eq. (2):

$$\text{Water absorption}\ (\%) = \left(W_f - W_0\right)/W_0 \times 100 \quad (2)$$

This determination was performed in triplicate for each type of sample, and the results were expressed as the arithmetic mean ± standard deviation.

The in vitro stability and degradation behavior of the sponges were evaluated based on their swelling degree in phosphate-buffered saline (PBS) and their weight loss over a period of 14 days. For each sponge formulation, three independent samples were cut into square specimens (4 cm^2) of uniform dimension and thickness. All samples were dried to a constant weight and individually weighed (W_0). For swelling tests, each specimen was immersed in 10 mL of PBS (pH 7.4) in sealed containers and incubated at 37 °C for 24 h. Excess PBS on the sponge surface was gently removed before determining the swollen weight (W_f). The swelling ratio was calculated according to Eq. (2). To evaluate degradation, the samples were incubated in PBS at 37 °C for 14 days. At predetermined time intervals (1, 3, 7, 10 and 14 days), specimens were removed, rinsed with distilled water to remove residual salts, and dried to a constant weight. Degradation was expressed as the percentage of weight loss relative to W_0 at each time point. Pure CNF sponges were included as control group.

2.4.2. Mechanical properties

The study of mechanical properties included compression and tensile strength analyses.

The compression tests for dried sponges and for wet sponges after water soaking were performed on an Instron LF Plus Lloyd Instrument testing machine equipped with a 1 kN load cell. Sponge test samples were prepared as cylinders of approximately 12 mm height and 25 mm diameter. They were placed between a pair of fixed plates (110 mm ø). Compression strength, Young's modulus and stress-strain curves of the samples were determined at a strain rate of 2 mm/min with a maximum strain limit of 80 %. The mechanical properties were evaluated in triplicate for each sponge, and the data were expressed as the arithmetic mean with its standard deviation.

Tensile tests were performed using the same equipment. The materials were made into films using the casting method and then cut into strips (1.5 × 10 cm). Tests included both dry and wet films after water soaking, and tensile strength, Young's modulus, and deformation were studied, in accordance with the ASTM D882 standard method [22]. Film strips were then fixed between the jaws with an initial separation of 65 mm, and the crosshead speed was set to 50 mm/min with a load cell of 1 kN. The results were expressed as the average of eight samples for each film.

Prior to measurements, all sponges and films were equilibrated at 25 °C and 50 % relative humidity (RH) according to the standard method.

2.5. Active properties of the sponges

2.5.1. Wound exudate uptake

To determine the ability of sponges to absorb wound exudate, layers mimicking skin were created as reported by Rostamitabar et al. [23]. A layer mimicking the dermis and a lower layer mimicking the hypodermis were used as a model of artificial skin to prevent excessive drying over time. The hypodermis was formed with gelatin (2 % w/w) and agar (0.4 % w/w) under agitation at 50 °C until a homogeneous solution was obtained, which was then poured into round Petri dishes to a height of 15 mm and allowed to solidify. The dermis layer was prepared in an analogous manner with gelatin (24 % w/w) and agar (2 % w/w) by pouring it over the hypodermis layer to a thickness of 5 mm. Once the layers were solidified, square pieces of the sponges (4 cm^2) were placed on top of the upper layer and covered with the lid of the plates. These plates were kept in a climatic chamber under controlled conditions of humidity (50 % RH) and temperature (25 °C) and the weight of the sponges was measured at 8 different time points up to 48 h. The wound exudate absorption capacity was expressed as the percentage of weight gain of the sponges. The tests were performed in triplicate.

2.5.2. Hemolysis test

To assess hemolysis activity, triplicates of the cutouts from the sponges were tested in accordance with the ISO 10993-4 standard [24]. Fresh sheep blood (less than 24 h old from collection, from Håtunalab AB, Sweden), was centrifuged at 2000 rpm for 10 min. The resulting supernatant was removed, and the remaining erythrocytes were washed three times with a normal saline solution. Subsequently, the erythrocytes were diluted to a concentration of 2.5 % in normal saline.

To the samples, first 200 μL of normal saline and then 800 μL of the diluted cell solution were added (final cell concentration of 2 %), followed by incubation for one hour at 37 °C. The samples were then subjected to centrifugation at 1500 rpm for 5 min. The absorbance of the supernatant was then measured at 540 nm (Varian Cary 50 Bio UV–Visible Spectrophotometer, USA). Normal saline and 1 % triton-X solutions were used as the blank and positive control, respectively. The percentage of hemolysis activity was calculated using the Eq. (3):

$$\%\text{Hemolysis} = (A_S - A_B)/(A_C - A_B) \times 100 \quad (3)$$

where, A_S, A_C and A_B are the absorbance of each sample, the positive control, and the blank, respectively.

2.5.3. Cytotoxicity assay: skin compatibility

The skin compatibility of the sponges was evaluated using HaCaT cells (keratinocyte cell line [25] Cell Lines Service, Eppelheim, Germany). The assessment was performed using the PrestoBlue® Cell Viability Reagent (Thermo Fisher Scientific, NO), a resazurin-based assay that measures metabolic activity as an indicator of cell viability [26].

HaCaT cells were cultured in Dulbecco's Modified Eagle Medium (DMEM) supplemented with 1 % Pen-Strep, 1 % glutamine, and 10 % fetal calf serum. The incubation conditions were maintained at 37 °C, 5 % CO_2, and 100 % humidity. A total of 11,000 cells per well were seeded in a 48-well plate. Circular pieces (Ø 0.5 cm) were cut from each sponge sample (CNF, CNF:G-ME, CNF:G-M, and CNF:G-E) and sterilized in absolute ethanol overnight. Subsequently, the samples were washed three times with PBS and incubated in the culture medium to prepare extracts at 50, 100, 200, and 400 mg/L.

The resulting sponge extracts were added to the respective wells and incubated for 24 h or 48 h. Each concentration and time point was tested in four technical replicates ($n = 4$) to ensure reproducibility.

After each incubation period, cell viability was determined using the PrestoBlue assay. The culture medium was replaced with fresh DMEM containing 10 % (*v*/v) PrestoBlue reagent, and the plates were incubated for 30 min at 37 °C. Fluorescence was measured at 560 nm excitation and 590 nm emission using a microplate reader (FLUOstar Omega, BMG Labtech, Germany).

The results were expressed as the percentage of viable cells relative to untreated controls. A 2 % Triton X-100 solution in culture medium was used as a positive control for cytotoxicity. All samples were analyzed within the same experimental setup to avoid variability related to cell passage or handling conditions.

2.5.4. Antimicrobial capacity

The antimicrobial activity of the foam composite was evaluated against *Bacillus cereus* (CCUG 7414), *Escherichia coli* (CCUG 10979) and *Staphylococcus aureus* (CCUG 10778, representing Gram-positive and Gram-negative bacteria, using the colony-counting method. Bacterial inoculates were prepared in Mueller Hinton Broth by incubating bacterial colonies at 37 °C for 24 h. The optical density at 600 nm was then adjusted to match the McFarland 0.5 standard (~10^8 CFU mL^{-1}). Foam samples (2 mg) were UV-sterilized on both sides and placed in sterile microplates containing 200 μL of Mueller Hinton Broth inoculated with 10^5 CFU mL^{-1} of bacterial culture. The plates were incubated at 37 °C for 24 h, after which 100 μL aliquots from serial dilutions were spread on Mueller Hinton Agar plates. All samples were tested in triplicate. Colony numbers were counted following 20 h of incubation at 37 °C, and bacterial growth inhibition was calculated relative to a control culture without foam samples.

2.6. Statistics

All data have been presented as the average ± standard deviation. Statistical analysis was done through analysis of variance (ANOVA) followed by Duncan test. Different letters show significant differences ($p \leq 0.05$).

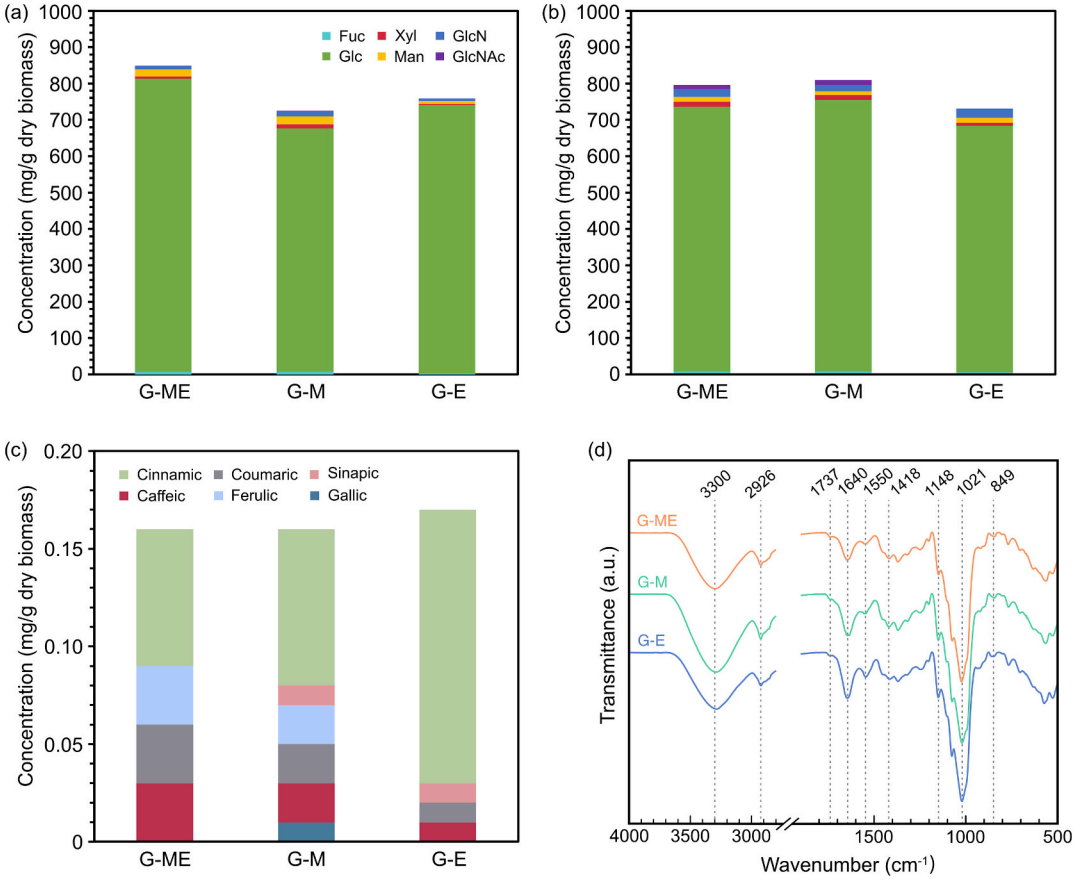

Fig. 1. Monosaccharide composition of the fungal biomass subjected to A) TFA hydrolysis and B) Sulfuric acid hydrolysis. C) Phenolic acid content and D) FTIR spectra of fungal biomasses.

3. Results and discussion

3.1. Characteristics and properties of G. lucidum-fungal biomass

The composition of the different *G. lucidum* fractions - G-ME, G-M and G-E - was analyzed by acid hydrolysis to determine their monosaccharide profiles. Samples were subjected to hydrolysis with either TFA and sulfuric acid prior to analysis (Fig. 1a and b). In all cases, glucose (Glc) was identified as the predominant monosaccharide, in agreement with previous reports for purified *G. lucidum* mycelium [13]. Consistent with literature, *G. lucidum* cell wall polysaccharides are mainly branched β-glucans, composed of β-D-(1➔3)(1➔6) [27].

In addition to Glc, two monosaccharides related to chitin were detected: glucosamine (GlcN) and *N*-acetyl-D-glucosamine (GlcNAc). Their presence supports the characteristic structure of fungal mycelium, where chitin is the main crystalline polysaccharide, with β-glucans forming the outer layer of the cell wall [11]. Other sugars, such as fucose, mannose and xylose, were present in much smaller amounts. Hydrolysis with sulfuric acid (Fig. 1b) resulted in a slightly lower overall carbohydrate content, reflecting more efficient breakdown of the crystalline polymers such as chitin (Table S2). In contrast, in the G-E fraction, composed mainly of EPS, milder hydrolysis with TFA preserved a higher carbohydrate yield, indicating less extensive degradation of polysaccharides.

The results also suggest interactions between the mycelium and EPS in the G-ME complex, as evidenced by the lower soluble protein content (Table S1). The phenolic acid profiles of the three fractions are shown in Fig. 1c. Cinnamic acid was the predominant compound, particularly in the purified G-E fraction. Ferulic, coumaric and caffeic acids were also identified, although in lower concentrations (Table S3). These phenolic acids may increase the antioxidant potential of the fractions. In addition, cinnamic acid derivatives have been reported to inhibit the growth of harmful bacteria such as *E. coli*, while preserving certain resistant lactic acid bacteria [28], a property of potential interest for applications in wound dressing.

The phenolic acid composition observed was consistent with that described by Dong et al., (2019) for *G. lucidum*. Their study highlighted the influence of drying techniques on the phenolic content of fungal biomass, identifying freeze-drying – the method used in this study - as the most effective for preserving compounds [29].

The identification of the characteristic chemical groups in the FB samples was determined by FTIR analysis (Fig. 1d). The broad band observed at 3300 cm^{-1} is usually related to the -OH groups of polysaccharides. The observed peak at 2926 cm^{-1} is indicative of the stretching vibrations of C—H, suggesting the presence of the CH_3 functional group [30]. The peak at 1737 cm^{-1} is due to the carboxyl ester group, which corroborates the presence of chitin base polymers in these FB. The peaks at 1640, 1550 and 1418 cm^{-1} indicated the C═O vibration, the N—H deformation of amide II and C—H bending vibrations of carboxylic and CH_3 and/or CH_2 functional groups, respectively. Finally, peaks at 1148, 1021 and 849 cm^{-1} are typical of β-glucans [14].

3.2. Physical and chemical characterization of CNF/FB-based sponges

Once the composition of the *G. lucidum* fractions was determined, CNF-based sponges enriched with these fractions were produced. Materials intended for wound dressing must effectively absorb blood and wound exudate to promote clotting and maintain a balanced moist environment. For this reason, porosity and water absorption capacity are critical parameters, as the most effective dressings are sponge-like. The ideal porosity of a hemostatic sponge-type material is considered to be at least 90 % [31].

Bulk density and porosity results are shown in Fig. 2a and b. The incorporation of FB led to a significant decrease in density (in the range of 7–8 mg/cm^3), compared to pure CNF sponge (11 mg/cm^3). At the same time, porosity increased to above 99 % in all FB-containing

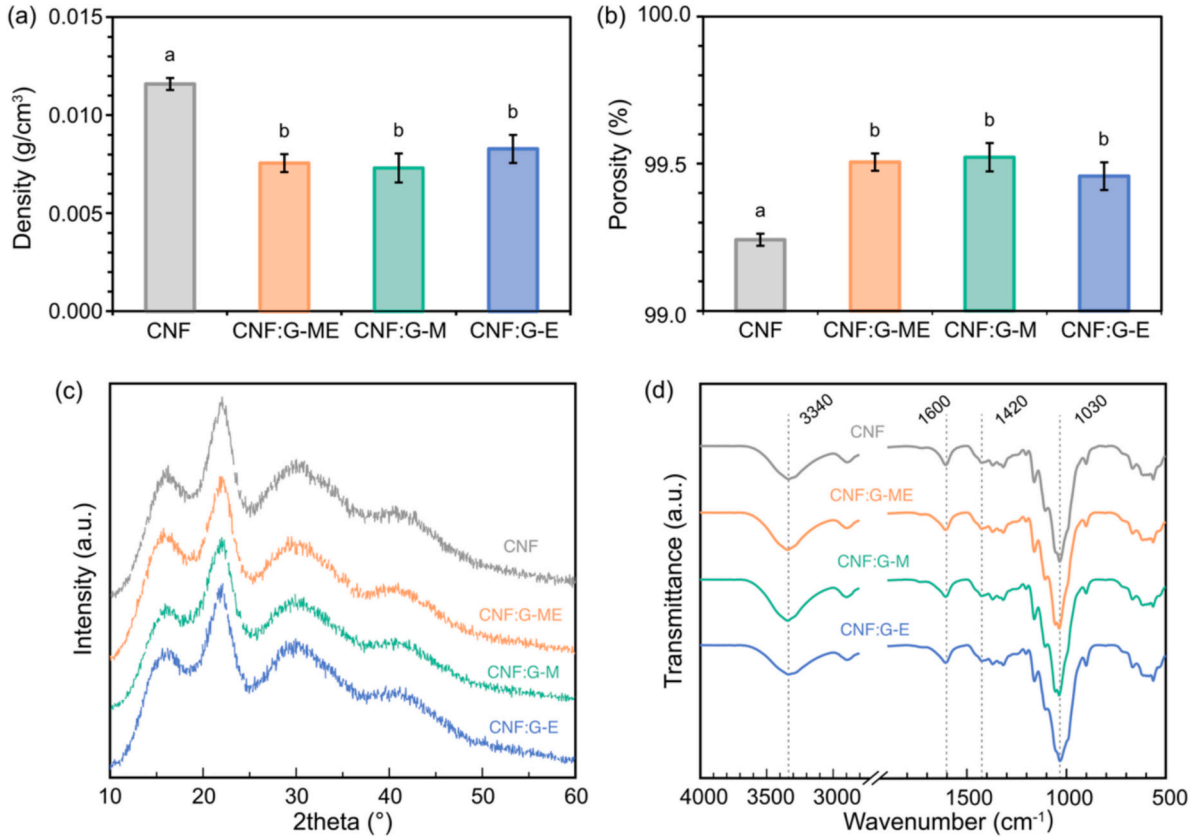

Fig. 2. (a) Density, (b) porosity, (c) XRD-patterns and (d) FTIR spectra of CNF-based sponges.

sponges, regardless of fraction type, with no significant differences between them. These values are consistent with aerogels described in CNF- and collagen-based tissue engineering applications [31]. The high porosity can be explained by the hydrophilic nature of the polysaccharide chains. When fungal biomass is added, its hydrophilic chains retain more water during the freezing process. This promotes the formation of larger or more structured ice crystals, which after freeze-drying results in a more open pore network [31]. This more open and connected network translates into a greater volume of accessible pores and, therefore, an increase in specific surface area (SSA), as confirmed by BET analysis: the SSA increased from 3.93 ± 0.04 m^2/g for pure CNF sponges to 5.39 ± 0.09 m^2/g for CNF:G-M, 6.66 ± 0.10 m^2/g for CNF:G-E and 7.39 ± 0.04 m^2/g for CNF:G-ME. These results indicate that the incorporation of FB not only improved porosity but also expanded the internal network, effectively increasing the available adsorption sites. Similar trends have been reported for cellulose aerogels with different alkali and alkaline earth metal chlorides. The increase in SSA was attributed to the addition of certain agents to the polymer matrix of the sponges leading to a "nanostructural reorganization" of the cellulose [32]. A higher SSA suggests a more open structure with improved fluid absorption capacity. It is important to note that, compared to commercial wound dressings such as polyurethane foams, the porosity of the present CNF-based sponges (>99 %) was substantially higher. Liu et al. (2017) reported porosity values ranging from 70 to 80 % for commercial foams [32].

The XRD patterns are shown in Fig. 2c. The absorption peaks in FB sponges were very similar to those in bulk CNF. Characteristic CNF peaks were found at $2\theta = 16.2°$ and $2\theta = 22.1°$ corresponding to the (110) and (200) crystalline planes typical of the crystal I type of cellulose [33]. A few small reflections observed at 30° and 40° denote the crystalline phase representing trace elements and compounds in the raw wheat straw cellulose fiber used to produce CNF [34]. Regarding the FTIR spectrum of the sponges, the neat CNF sponge showed the characteristic peaks at 3340, 1600, 1420 and 1030 cm^{-1} corresponding to the vibration of OH groups, C═O stretching of carboxyl groups, CH_2 groups and to the carbonyl bonds of the cellulose skeleton, respectively [35]. When FB were added no new peaks were observed. This is due to two reasons: (i) the FTIR spectra of CNF and FB are very similar as the most characteristic peaks of both samples overlap and (ii) the interaction between CNF and FB does not generate new functional groups, suggesting that mainly hydrogen bonds are formed between these components. A similar observation was reported by Zhang et al. (2023) for banana pseudo-stem nanocellulose aerogels enriched with konjac glucomannan [36].

The morphology of the fabricated biomaterials was investigated by SEM (Fig. 3). The SEM images revealed that the sponges structurally resembled polyurethane (PU) foam dressings and biomaterial-based skin scaffolds, such as those incorporating collagen [37]. A study by Heit et al. examined PU foam dressings with pore sizes ranging from 0.7 to 3.1 mm, assessing their function as interface materials for suction devices. That work emphasized the critical role of dressing pore size in wound healing, suggesting that foams with smaller pores are better suited for highly proliferative wounds, as they help prevent undesirable foam ingrowth [38].

In terms of pore size, sponges exhibited a non-homogeneous structure compared to industrially manufactured PU foams. However, when FB was introduced to the CNF composition, a structure with a greater number of pores, which were also more uniformly sized, was obtained. SEM-derived statistical histograms of the pore size distribution are shown in Fig. 4. The morphology of the CNF, CNF:G-ME, CNF:G-M, and CNF:G-E sponges showed a macroporous structure with APS values of 96.97, 94.58, 90.77, and 99.56 μm, respectively. The size distribution of most pores ranged from 25 to 275 μm, 25 to 225 μm, 25 to 325 μm, and 25 to 275 μm for CNF, CNF:G-ME, CNF:G-M, and CNF:G-E sponges, respectively. Among the sponges, the one incorporating G-ME (Fig. 3b) displayed the most homogeneous structure, with the narrowest pore size distribution (Fig. 4b). Notably, this sample also exhibited the highest SSA, suggesting a greater fraction of accessible pore surfaces, which may benefit from its improved structural uniformity. According to Yannas et al. [39] the optimal pore size for artificial skin grafts that facilitate cell penetration falls within the range of 50–150 μm. The APSs observed in the present sponges (around 90–100 μm) align with the higher end of this range and are comparable to the pore size of artificial skin produced by Cahn et al. (115–120 μm) [37]. In comparison to commercial foam dressings [40], the CNF/FB-based sponges exhibited pore sizes similar to those of Medifoam®N, albeit with slightly greater variation. The thickness of the pore wall in the current sponges (less than 0.1 μm), relative to the pore size, was substantially lower than the PU foam dressing [39]. This parameter plays a pivotal role in determining the mechanical properties and flexibility of a foam [41].

Water absorption capacity is one of the most critical parameters for wound dressing applications, as these must effectively remove wound exudate while preventing bacterial colonization [42,43]. The water absorption capacities of the sponges are shown in Fig. 5a. The pure CNF sponge showed an absorption capacity of 7600 %. The inclusion of FB altered this behavior depending on the fraction used. The CNF:G-M sponge showed a notable increase, reaching 9200 %. In contrast, the addition of the more purified EPS fraction (G-E) reduced water absorption to 6100 %. However, all sponges maintained high absorbency (>4000 %), providing sufficient surface area and liquid retention to be considered suitable for wound dressing applications. The values were consistent with those reported previously for Janus nanofiber-based porous materials [4] and significantly exceeded those of commercial polyurethane-based foams, such as CaduMeti, which have water and saline absorption capacities of 1330 and 1367 %, respectively [32]. Therefore, sponges obtained in the present study represent a four- to seven-fold improvement in fluid management performance compared to current marketed products.

To evaluate their swelling and stability under physiological conditions, the sponges were immersed in PBS. The swelling ratio after 24 h is shown in Fig. 5b. The lower swelling of CNF:G-M and CNF:G-E compared to pure CNF is likely due to stronger intermolecular interactions and partial ionic cross-linking between polysaccharide chains and phosphate ions in PBS, which limits network expansion [44]. These findings suggest that the incorporation of fungal biomass modulates the hydrophilic-hydrophobic balance and polymer-ion interactions, resulting in tunable swelling behavior desirable for exudate management control. The in vitro degradation profile of the sponges in PBS over 14 days (Fig. 5c) revealed different stability trends depending on the fraction incorporated. The CNF:G-ME and CNF:G-M samples showed a faster initial mass loss (up to 25 % in the first 3 days), followed by stabilization, while the CNF:G-E and pure CNF samples showed gradual, almost linear degradation. The greater initial degradation of sponges containing mycelium may be related to their higher absorption capacity (Fig. 5a). This can be attributed to their lower tendency to form hydrogen bonds with CNF, together with the presence of bound phenolic acids. In particular, gallic acid, which contains multiple -OH groups, likely improves water retention by facilitating interactions with surrounding water molecules. In contrast, the denser network of CNF:G-E and CNF restricted fluid diffusion, providing greater structural integrity over time. These results demonstrate that the degradation rate of CNF-based sponges can be adjusted by the type of fungal biomass incorporated, an essential property for wound dressings, where gradual resorption of material and its replacement by regenerated tissue is desirable [45]. This controlled degradability may be advantageous for tailoring the material resorption rate to tissue regeneration dynamics.

As a wound dressing, the material is inevitably subjected to various stresses during application. Therefore, good compressive strength and adequate softness are required to maintain sponge integrity and prevent secondary wound damage [46]. The pure CNF sponges were relatively flexible in the dry state, with compression strength values similar to those previously reported by the research group for these materials [35].

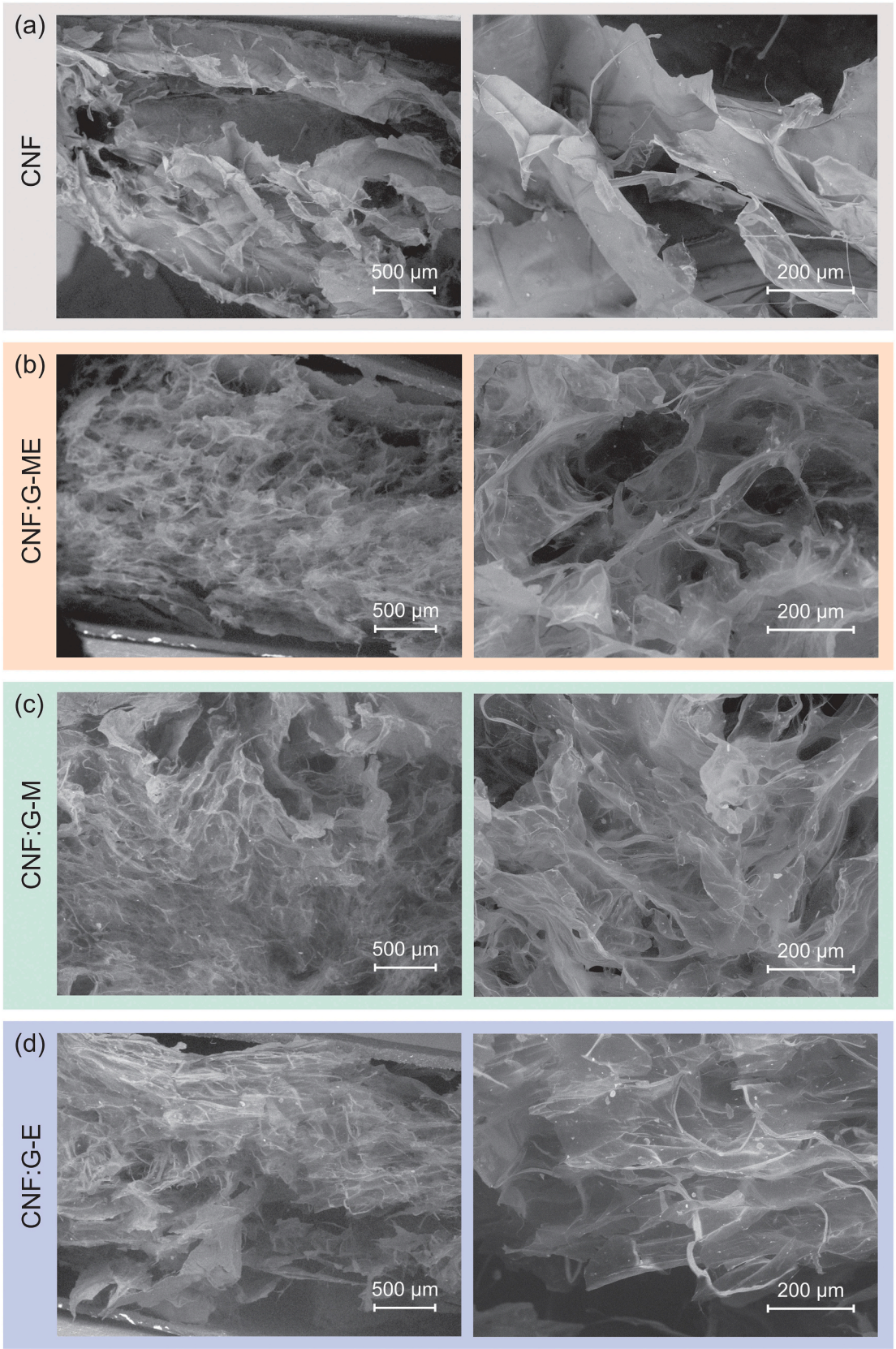

Fig. 3. SEM images of (a) CNF, (b) CNF: G-ME, (c) CNF: G-M, and (d) CNF:G-E sponges.

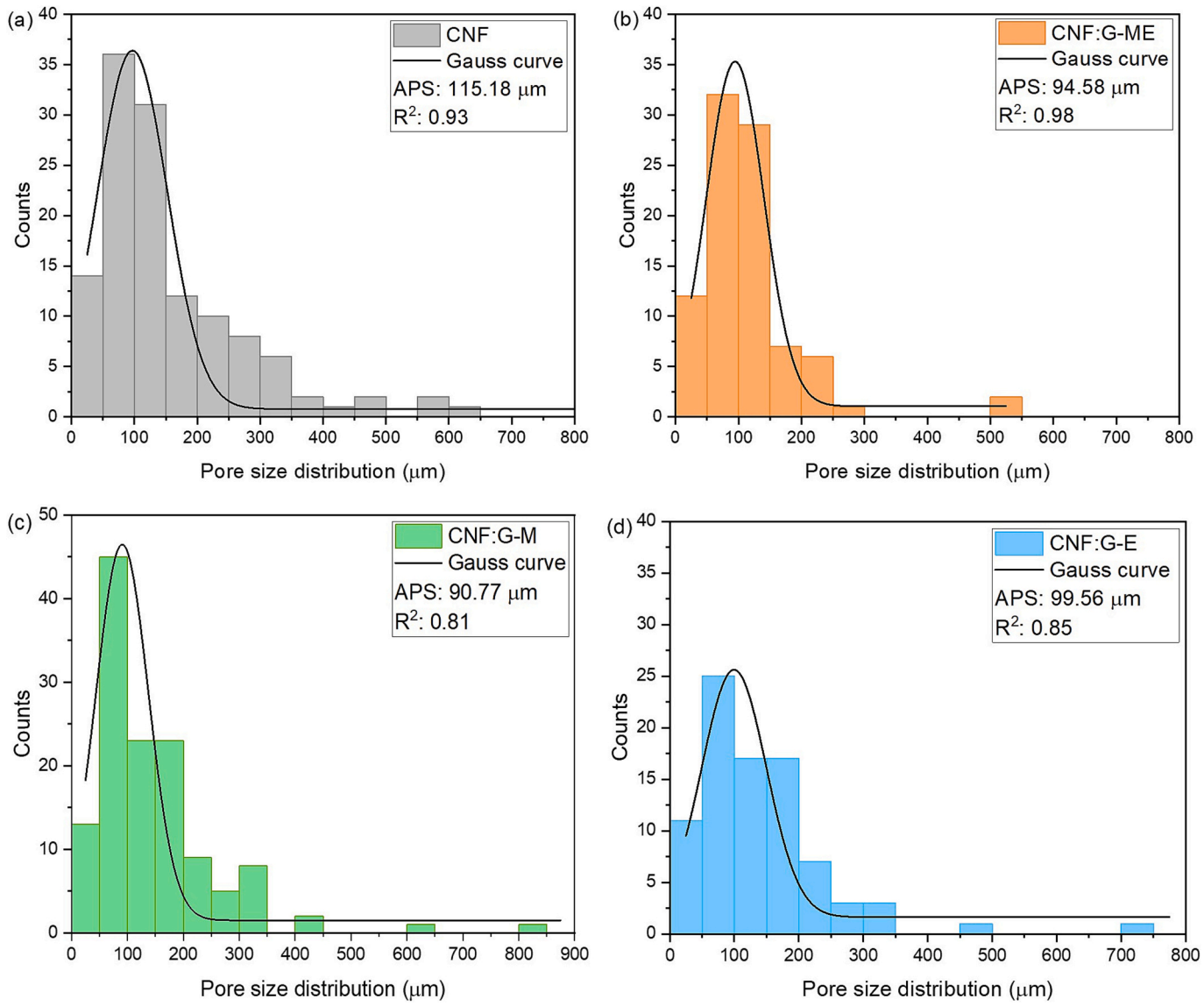

Fig. 4. Statistical histograms of the pore size distribution derived from the SEM micrographs. The Gauss curves indicate the APS of the data.

In addition, they maintained their shape well when hydrated. Incorporation of different FB fractions did not impair these properties and even enhanced them. The stress-strain curves of the sponges are shown in Fig. 6. Three deformation stages can be distinguished in these curves. In the first stage (up to 20 % deformation), linear elastic deformation of the cellulose structure and collapse of the macropores occur when subjected to low stresses. The curve then rises slowly due to the onset of plastic deformation, in which the porous network undergoes irreversible structural changes after exceeding the elastic limit. In the third region (deformation greater than 80 %), the stress increases dramatically due to densification caused by bending or damage to the mesopores, as well as compression and rupture of intermolecular interactions between the fibers [35].

These effects were more pronounced in sponges containing mycelium-rich FB fractions. Compressive strength and Young's modulus are summarized in Table 1. Sponges with the G-M fraction exhibited the highest compressive strength (14.49 kPa) and modulus (142.25 kPa). In general, the addition of FB fractions increased the compressive strength of CNF sponges (Fig. 6a). The mechanical response of wet sponges showed a similar trend to that of dry ones. The reduced modulus in the hydrated state provided excellent softness (Fig. 6b), as free water acts as a plasticizer for natural polymers, enhancing flexibility. Although no significant differences were observed between the Young's moduli of wet samples (Table 1), all values were comparable to that of human skin (around 5 kPa) [46]. The superior compressive properties of the CNF:G-M sponge are likely due to the combined effect of (i) rigid chitin-glucan fragments from the mycelium acting as reinforcing fillers [47], (ii) a smaller average pore size and favorable pore size distribution allowing for more uniform stress distribution [48], and (iii) better fiber contacts and pore wall architecture that improve load transfer [49].

However, it is known that density has a direct relationship with the mechanical properties of CNF-based materials [35]. Therefore, to eliminate the effect of this variable given the high variation in density between samples (Fig. 2a), the specific compressive strength (specific CS) and specific Young's modulus (specific YM) were calculated for the sponges (Table 1). Clear effects of FB inclusion on the mechanical performance of the materials were observed. Thus, the addition of any of the *G. lucidum* fractions significantly improved the compressive strength of the sponges, both dry and wet. However, no clear differences were observed between the inclusion of different fractions, highlighting the strong effect of density on these properties. This confirms that the improved mechanical response cannot be solely attributed to density differences but also to reinforcement from the fungal components.

In addition to compression, the tensile mechanical properties of the

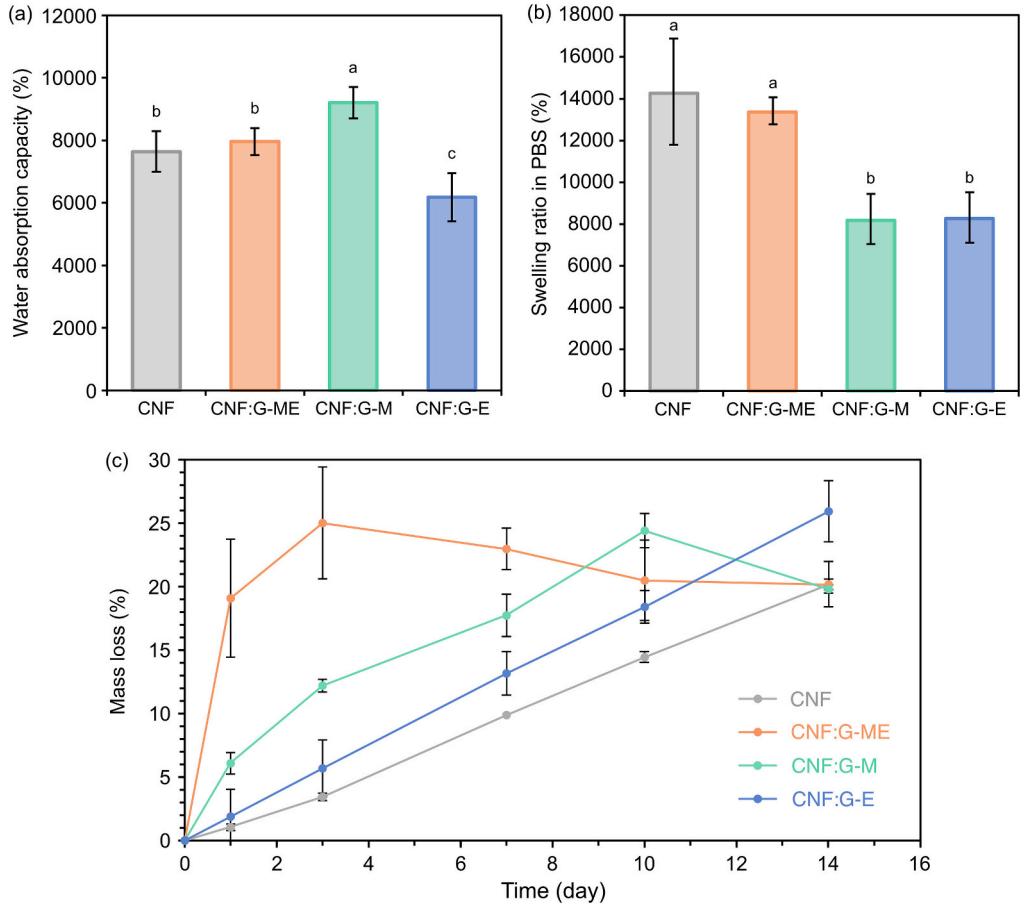

Fig. 5. Water absorption capacity (A), swelling ratio in PBS (B) and in vitro degradation (C) of CNF-based sponges enriched with different fungal-derived biomass. *Results are expressed as the mean of three repetitions (n = 3) with their standard deviation.*

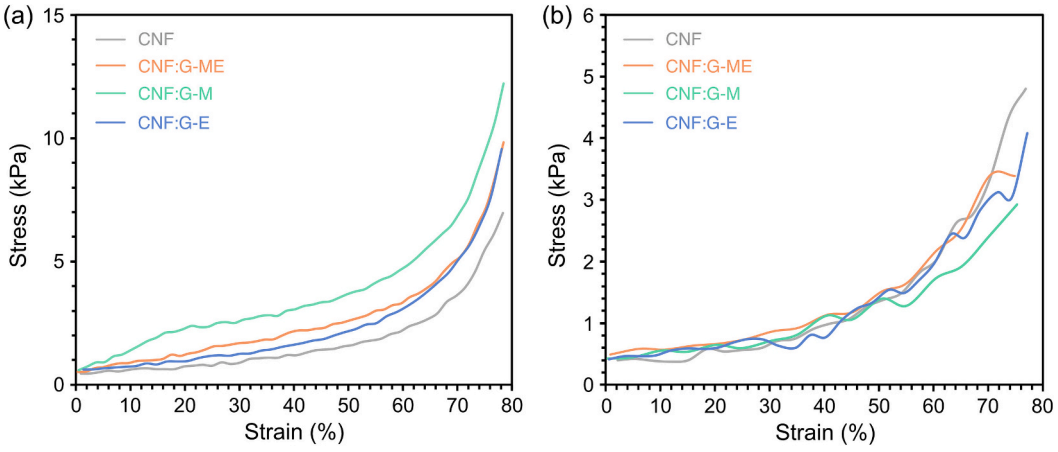

Fig. 6. Compressive stress-strain curves of CNF-based sponges enriched with different fungal-derived biomass under dried state (A) and wet state (B).

materials were investigated in both dry and wet states. The results obtained are shown in Fig. 7. CNF:G-ME had the highest tensile stress (TS) of 30.06 MPa (Fig. 7a). CNF:G-M and CNF:G-E showed lower TS. However, these values are very similar to those reported for polyurethane films applied in negative pressure wound therapy [50]. When wet, the values obtained for all samples decreased, as was the case with the sponges. As mentioned above, water acts as a plasticizer with natural polymers. A very significant increase in the elongation at break of the wet samples was observed (Fig. 7b). In other words, contact with water increased their flexibility. The CNF:G-M sample provided the highest elongation (3.49 mm). This fraction had the highest water absorption capacity, which could be related to its greater flexibility. In tensile tests, strength and deformation are inversely proportional. More resistant materials are less deformable and therefore exhibit lower elongation, as observed in the results obtained. These mechanical values are in line with or even exceed those reported for other biopolymeric systems based on PVP/CNF/*Aloe Vera* electrospun composites [10].

Table 1
Compressive tests of CNF-based sponges enriched with different fungal-derived biomass in dry and wet states.

Groups		Compressive stress (kPa)	Young's modulus (kPa)	Specific CS (kPa·cm^3/g)	Specificc YM (kPa·cm^3/g)
Dry sponges	CNF	9.50 ± 1.24^{c}	133.75 ± 15.94^{a}	0.82 ± 0.11^{b}	11.54 ± 1.37^{c}
	CNF:G-ME	11.48 ± 0.70^{b}	109.90 ± 14.74^{a}	1.52 ± 0.09^{a}	17.13 ± 4.69^{b}
	CNF:G-M	14.49 ± 0.80^{a}	142.25 ± 10.67^{a}	1.79 ± 0.35^{a}	19.48 ± 1.46^{b}
	CNF:G-E	10.89 ± 0.75^{b}	127.24 ± 25.80^{a}	1.50 ± 0.32^{a}	28.94 ± 4.90^{a}
Wet sponges	CNF	5.66 ± 0.84^{a}	16.39 ± 4.36^{a}	0.49 ± 0.07^{c}	1.41 ± 0.38^{a}
	CNF:G-ME	$4.81 \pm 0.52^{a,b}$	17.30 ± 11.26^{a}	$0.64 \pm 0.07^{a,b}$	2.29 ± 1.48^{a}
	CNF:G-M	4.05 ± 0.25^{b}	19.66 ± 7.51^{a}	$0.56 \pm 0.03^{b,c}$	1.64 ± 0.45^{a}
	CNF:G-E	$5.07 \pm 0.97^{a,b}$	24.12 ± 4.47^{a}	0.68 ± 0.06^{a}	2.14 ± 0.55^{a}

*Different superscript letters indicate statistical differences ($p \leq 0.05$) between samples from the same group (dry or wet).

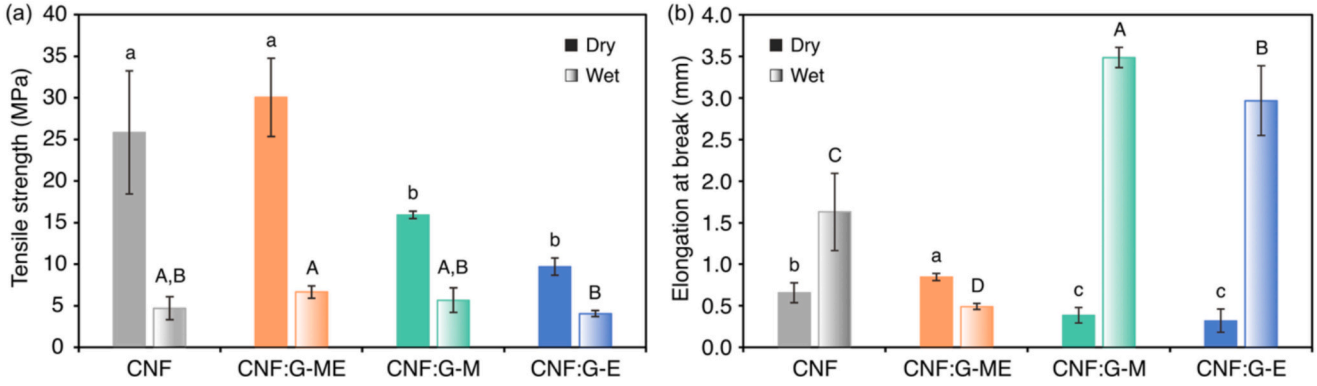

Fig. 7. Tensile strength (a) and elongation at break (b) of CNF-based sponges enriched with different fungal-derived biomass under dry and wet state. **Different letters above the bars (lowercase for dry samples, uppercase for wet samples) indicate statistical differences ($p \leq 0.05$) between samples from the same group.*

3.3. Active properties for wound healing applications

Using skin-mimicking layers, the absorption of wound exudate into the sponges was evaluated to simulate in vivo conditions (Fig. 8a). A very rapid uptake of exudate was observed within the first 2–3 h (reaching 170–240 %), after which the absorption rate slowed and stabilized until 48 h. Overall, total exudate uptake exceeded 400 %, remarkably high values than can be attributed to the outstanding water absorption capacity of the sponges, as previously discussed. The slightly lower uptake compared to pure water absorption can be explained by the restricted water diffusion across the gelatin-agar interface of the skin-mimicking system.

The exudate absorption values of CNF/FB sponges were considerably higher than those reported for cellulose-chitosan microfiber aerogels and comparable to those of CNF or bacterial cellulose aerogels [23,51]. In line with water absorption behavior, some differences emerged between FB fractions. Sponges containing G-M and G-E fractions showed faster absorption during the first 24 h compared to pure CNF, although they reached similar equilibrium values. In contrast, CNF:G-ME sponges showed faster and higher overall exudate absorption, likely due to their larger surface area, which facilitated liquid penetration and retention. This superior absorption performance highlights the potential of CNF-based sponge dressings to provide effective exudate control while maintaining structural integrity during application. Taken together, the adjustable structure, fluid management capacity, and mechanical strength of CNF/FB sponges establish a promising basis for further evaluation of their biological and antimicrobial performance.

Blood compatibility is an important factor in materials intended for hemostasis in clinical settings [52]. As per the findings reported by Fazley Elahi et al. [53], compounds exhibiting hemolysis activity below 2 % are classified as non-hemolytic, while compounds demonstrating hemolysis activity in the range of 2–5 %, and greater than 5 %, are categorized as slightly hemolytic and hemolytic, respectively. Hemolytic activity allows for a simple, efficient, and reliable evaluation of the hemocompatibility of biomaterials. According to ASTM F756-17 standard, biomaterials with less than 5 % hemolysis have better compatibility with blood [54]. Based on the results of the present study, the sponges showed hemolytic effect values between 0.15 and 0.91 % with

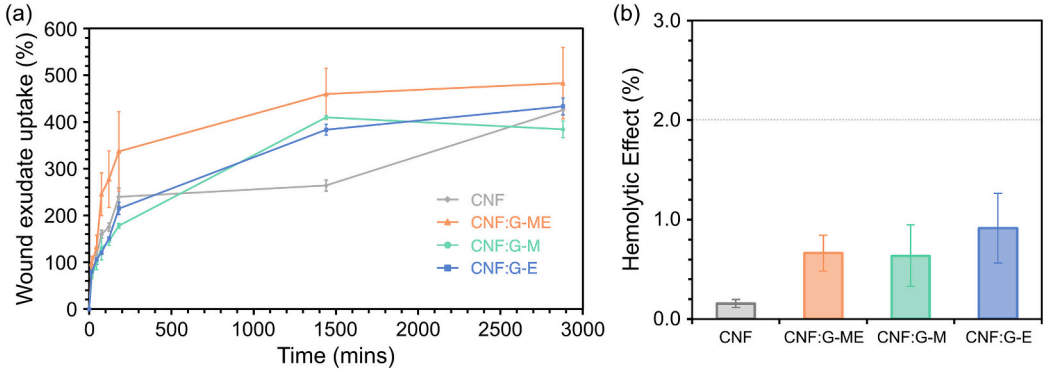

Fig. 8. (a) Wound exudate uptake (%) of CNF/FB-sponges under skin-mimicking conditions. (b) Hymolytic effect of CNF/FB-sponges.

the control CNF sponge being the least hemolytic one, followed by the sponge containing G-M (Fig. 8b). All sponges had minimal hemolytic effect and therefore were cleared as non-hemolytic. In comparison with CNF/silver nanoparticles – chitosan pads produced by Zaitun Hasibuan et al. [55], the current ones have even lower hemolytic effect and can be considered excellent candidates for wound dressing.

Cytotoxicity test results to evaluate the skin cells compatibility of the prepared sponges are also displayed in Fig. 9. The evaluation was performed using the PrestoBlue® resazurin-based assay at four different concentrations (50, 100, 200, and 400 mg/L) and two incubation times (24 and 48 h). At all tested concentrations and timepoints, the cell viability remained above 90 %, confirming that the materials are non-cytotoxic according to the ISO 10993-5:2009 standard [24]. The untreated HaCaT cells served as the negative control (100 % viability), while 2 % Triton X-100 was used as the positive control to validate assay responsiveness. Among the tested formulations, the FB-enriched sponges demonstrated slightly higher viability compared to the pure CNF material, suggesting a positive contribution of fungal biomass components, particularly the EPS, to the overall biocompatibility of the composites. In addition, further in vitro and in vivo assays could be conducted to evaluate the effect of FB on the rate of healing in acute and chronic conditions to gain an expanded perspective on its application as wound dressings. Compared to the study of Kempf et al. [56], who tested cytotoxicity of various wound dressing on HaCaT cells, the materials developed in this study demonstrated equal or superior cytocompatibility, with cell viability consistently exceeding 90 %, surpassing the performance of products such as Bactigras, Acticoat and ConvaCare wound dressing. The current sponges are also comparable to flamazine, with similar cell viability effect on HaCaT [57].

The antimicrobial activity of the foam composites was evaluated against *B. cereus*, *E. coli*, and *S. aureus* using the colony-counting method. The results (Fig. S1) showed that the tested materials did not significantly inhibit the growth of *B. cereus* or *E. coli*, indicating limited activity against these bacterial strains. However, a distinct bactericidal effect was observed against *S. aureus* for the CNF:G-E and CNF:G-ME samples. These two formulations contained the EPS fraction derived from the fungal biomass, suggesting that the presence of EPS contributes to the antimicrobial properties of the composites.

Given that *S. aureus* is one of the predominant pathogens associated with skin and wound infections, this selective inhibition of Gram-positive bacteria is particularly relevant for wound-healing applications [58]. Importantly, the inclusion of EPS not only enhanced antibacterial performance but did so without compromising the mechanical properties of the foams and, in the case of CNF:G-ME, even resulted in a higher wound exudate uptake capacity. This indicates that complete removal of EPS from the fungal biomass is unnecessary, as its retention improves the overall functionality of the material by combining biocompatibility, mechanical integrity, fluid absorption capacity, and targeted antimicrobial potential. These findings reinforce the suitability of the CNF-based sponges as advanced bioactive wound dressing candidates.

As previously mentioned, several CNF-based biomaterials have been investigated in the literature for wound dressing applications. The key characteristics of these materials, in comparison with those developed in the present study, are summarized in Table 2. This comparison highlights the excellent water uptake capacity of CNF sponges enriched with different *G. lucidum* fractions, confirming the suitability of this architecture for efficiently absorbing fluids and treating heavily exuding wounds. These results are further supported by the low hemolytic activity observed, indicating the material's biocompatibility for biomedical use. The lower mechanical strength observed for the present biomaterials compared with other CNF-based systems can be attributed to their lower density. The CNF sponges containing *G. lucidum* EPS are the lightest among those reported, and it is well established that increasing the solid content during biomaterial formulation proportionally enhances mechanical strength [35]. Nevertheless, it is worth noting that comparable functional performance was achieved using significantly less material. Moreover, unlike sodium alginate/CNF sponges coated with a bio-polyurethane, as reported by Yadav et al. [58], the present sponges were uncoated, yet still exhibited satisfactory mechanical stability. Future work will focus on improving the mechanical properties by increasing the proportion of structural components, particularly *G. lucidum* polysaccharides, which are expected not only to reinforce the matrix but also to further enhance cytocompatibility.

4. Conclusion

The exopolysaccharides and mycelium from *G. lucidum* were successfully isolated and characterized, confirming their typical fungal cell

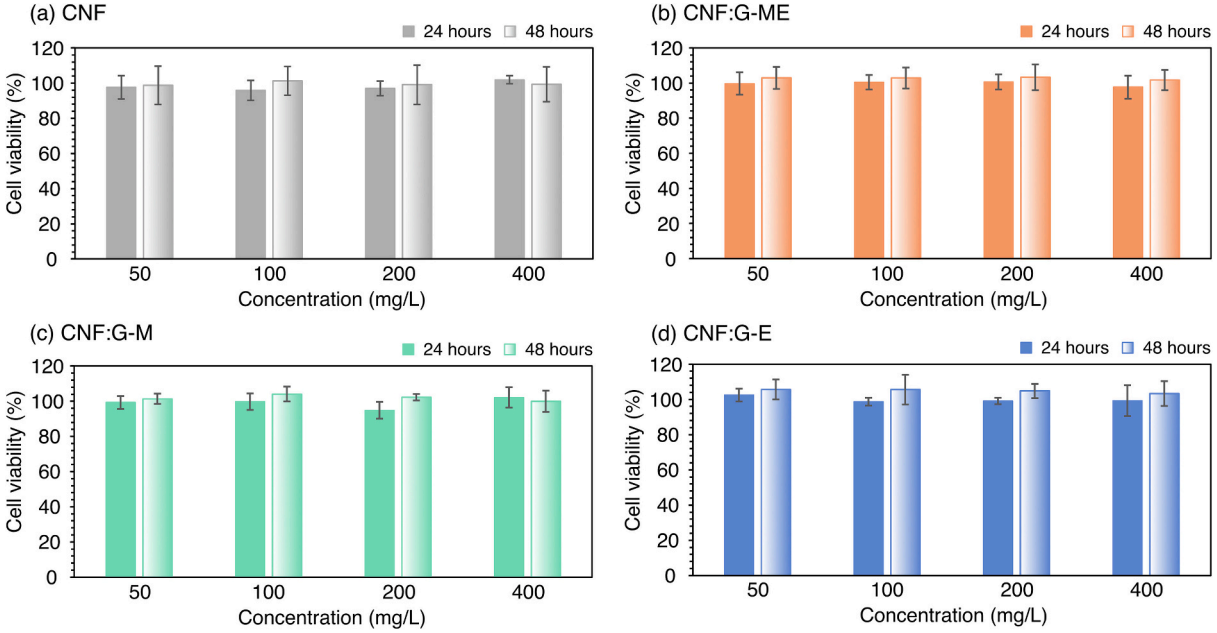

Fig. 9. Cytotoxicity test of the CNF-based sponges.

Table 2
Characteristics of several cellulose nanofiber-based porous biomaterials for wound dressing applications.

Biomaterial	Density (mg/cm^3)	Water uptake (%)	Compression strength (kPa)	Hemolytic effect (%)	Cell viability (%)	Ref.
CNF/*G. lucidum* fungal polysaccharides sponge.	7–8	9200	14.5	0.6	62.7	Current study
Quaternized chitosan-Carboxylated CNF sponge.	60–65	934	297	<3	>85	[60]
Carboxymethyl chitosan/CNF sponge.	40	3138	35–45	1.3–1.4	>100	[61]
Sodium Alginate-CNF sponge with bio-polyurethane coating.	920	1200	3800	0.4	100	[59]
Citric acid cross-linked Carboxymethyl CNF aerogel.	9–15	6600	3–4	1.4	>99	[62]
CNF/Chitosan aerogel	21.7	4440	75.4	1.6	97.3	[63]
CNF/Collagen/Chitosan aerogel.	15.6	7100	32	<1	70–90	[64]
Nanocellulose/Cinnamon extract sponge.	20–30	1435	37	<5	78–93	[65]

wall composition rich in β-glucans and chitin-derived polysaccharides. Phenolic acids, mainly derived from cinnamic acid, were also identified, which could contribute antioxidant and bioactive properties to the fungal fractions.

These components were incorporated into CNF-based sponges to evaluate their influence on the structure-property relationships of composite materials. The incorporation of fungal biomasses significantly reduced the bulk density, while increasing porosity to over 99 % and the specific surface area to 7.4 m^2/s. The effect depended on the type of fungal fraction used. The mycelium fraction (G-M) improved water absorption capacity (up to 9200 %) and compressive strength due to the reinforcing action of chitin-glucan fragments. The purified exopolysaccharide fraction (G-E) provided greater structural stability and slower degradation in physiological media. The combined mycelium and exopolysaccharide fraction (G-ME) produced the most homogeneous and interconnected pore structure, as well as the highest tensile strength.

All CNF sponges enriched with fungi showed excellent liquid absorption under conditions similar to those found in wounds, achieving up to 400 % exudate absorption, which significantly exceeds that of conventional polyurethane dressings. Their swelling and degradation profiles can be tailored by selecting the appropriate fungal fraction, offering adjustable reabsorption behavior desirable for wound healing applications.

This study demonstrates the successful development of CNF-based composite sponges incorporating Ganoderma lucidum biomass fractions. The results confirm that integrating *G. lucidum* biomass into CNF matrices can modulate structural and mechanical properties without compromising flexibility or integrity. This demonstrates that complete purification of the fungal material is not necessary to achieve functional improvement, thereby simplifying processing and reducing production costs.

The biological evaluation of these sponges, including hemocompatibility, cytotoxicity, and antimicrobial activity, further supports their potential as multifunctional wound dressings. In particular, the retention of EPS within the fungal biomass contributed positively to cell compatibility, fluid absorption, and selective antibacterial activity against *S. aureus*, highlighting their relevance for treating skin and wound infections.

Overall, the developed sponges combine biocompatibility, mechanical resilience, fluid management capacity, and antimicrobial functionality, positioning them as promising candidates for sustainable and effective wound dressing applications.

CRediT authorship contribution statement

Esther Rincón: Writing – review & editing, Writing – original draft, Validation, Methodology, Investigation, Formal analysis, Data curation, Conceptualization. **Maryam Nejati:** Writing – original draft, Investigation, Formal analysis, Data curation. **Li Zha:** Writing – review & editing, Writing – original draft, Validation, Formal analysis. **Eduardo Espinosa:** Writing – original draft, Validation, Supervision, Project administration, Methodology, Investigation, Funding acquisition, Formal analysis, Data curation. **Amparo Jiménez-Quero:** Writing – review & editing, Writing – original draft, Validation, Supervision, Project administration, Methodology, Investigation, Funding acquisition, Conceptualization.

Funding

The authors acknowledge the financial support provided by Consejería de Universidad, Investigación e Innovación (Junta de Andalucía, Spain) through AT21_00143 project. The authors acknowledge funding from the Knut and Alice Wallenberg Foundation (KAW) through the Wallenberg Wood Science Center, WWSC 3.0 (KAW 2021.0313); and from the Swedish Research Council Formas (Project 2022-00401) and the Carl Tryggers Foundation (Project 22:2169).

Declaration of competing interest

The authors declare the following financial interests/personal relationships which may be considered as potential competing interests: Amparo Jimenez Quero reports financial support was provided by Knut and Alice Wallenberg Foundation. Amparo Jimenez Quero reports financial support was provided by Swedish Research Council Formas. Amparo Jimenez Quero reports financial support was provided by Carl Trygger Foundation for Scientific Research. Eduardo Espinosa reports financial support was provided by Junta de Andalucía Consejería de Educación. If there are other authors, they declare that they have no known competing financial interests or personal relationships that could have appeared to influence the work reported in this paper.

Acknowledgments

The authors gratefully acknowledge the support of Dr. Zeinab Qazanfarzadeh for her valuable assistance with the antimicrobial assays and Dr. Marianne Dore Hansen for her support in conducting the cell biocompatibility experiments.

Appendix A. Supplementary materials

Tables S1 to S3. Numerical data of soluble protein content, total phenolic acid (TPC, Folin-Ciocalteu method, and Zeta potential of fungal derived biomass and cellulose nanofibers, monosaccharide composition of the fungal biomass after sulfuric acid or TFA hydrolysis tests and phenolic acids profile in fungal biomass-derived samples. Supplementary data to this article can be found online at https://doi.org/10.1016/j.ijbiomac.2025.149401.

Data availability

Data will be made available on request.

References

[1] A.E. Eldeeb, S. Salah, N.A. Elkasabgy, Biomaterials for tissue engineering applications and current updates in the field: a comprehensive review, AAPS PharmSciTech 23 (2020) 267, https://doi.org/10.1208/s12249-022-02419-1.

[2] A. Akhtar, V. Farzam Rad, A.-R. Moradi, M. Yar, M. Bazzar, Emerging polymeric biomaterials and manufacturing-based tissue engineering approaches for neuro regeneration-a critical review on recent effective approaches, Smart Mater. Med. 4 (2023) 337–355, https://doi.org/10.1016/j.smaim.2022.11.007.

[3] F.-C. Chao, M.-H. Wu, L.-C. Chen, H.-L. Lin, D.-Z. Liu, H.-O. Ho, et al., Preparation and characterization of chemically TEMPO-oxidized and mechanically disintegrated sacchachitin nanofibers (SCNF) for enhanced diabetic wound healing, Carbohydr. Polym. 229 (2020) 115507, https://doi.org/10.1016/j.carbpol.2019.115507.

[4] K. Zhang, X. Jiao, L. Zhou, J. Wang, C. Wang, Y. Qin, et al., Nanofibrous composite aerogel with multi-bioactive and fluid gating characteristics for promoting diabetic wound healing, Biomaterials 276 (2021) 121040, https://doi.org/10.1016/j.biomaterials.2021.121040.

[5] E. Mohamed, Y. Wang, P.J. Crispin, A. Fitzgerald, J.E. Dahlstrom, S. Fowler, et al., Superior hemostatic and wound-healing properties of gel and sponge forms of nonoxidized cellulose nanofibers: in vitro and in vivo studies, Macromol. Biosci. 22 (2022), https://doi.org/10.1002/mabi.202200222.

[6] D. Dong, R. Chen, J. Jia, C. Zhao, Z. Chen, Q. Lu, et al., Tailoring and application of a multi-responsive cellulose nanofibre-based 3D nanonetwork wound dressing, Carbohydr. Polym. 305 (2023) 120542, https://doi.org/10.1016/j.carbpol.2023.120542.

[7] H. Ao, K. Duan, D. Zhang, X. Xun, F. Feng, H. Liu, J. Li, Y. Li, Y. Wan, Biofunctionalized bacterial cellulose grafted with bacitracin for wound healing, J. Mater. Sci. 59 (2024) 10987, https://doi.org/10.1007/s10853-024-09819-7.

[8] H. Ao, W. Jiang, Y. Nie, C. Zhou, J. Zong, M. Liu, X. Liu, Y. Wan, Engineering quaternized chitosan in the 3D bacterial cellulose structure for antibacterial wound dressings, Polym. Test. 86 (2020) 106490, https://doi.org/10.1016/j.polymertesting.2020.106490.

[9] A.T.K. Basti, M. Jonoobi, S. Sepahvand, A. Ashori, V. Siracusa, D. Rabie, T. H. Mekonnen, F. Naeijian, Employing cellulose nanofiber-based hydrogels for burn dressing, Polymers (Basel) 14 (2022) 1207, https://doi.org/10.3390/polym14061207.

[10] M. Zand, S. Sepahvand, P. Khoshkhat, M. Chamani, M. Jonoobi, A. Ashori, Preparation and characterization of poly(vinyl pyrrolidone)/cellulose nanofiber/aloe vera composites as a biocompatible hydrating facial mask, Int. J. Biol. Macromol. 277 (2024) 133846, https://doi.org/10.1016/j.ijbiomac.2024.133846.

[11] M. Hamidi, O.V. Okoro, P.B. Milan, M.R. Khalili, H. Samadian, L. Nie, et al., Fungal exopolysaccharides: properties, sources, modifications, and biomedical applications, Carbohydr. Polym. 284 (2022) 119152, https://doi.org/10.1016/j.carbpol.2022.119152.

[12] I.C.F.R. Ferreira, S.A. Heleno, F.S. Reis, D. Stojkovic, M.J.R.P. Queiroz, M. H. Vasconcelos, et al., Chemical features of Ganoderma polysaccharides with antioxidant, antitumor and antimicrobial activities, Phytochemistry 114 (2015) 38–55, https://doi.org/10.1016/j.phytochem.2014.10.011.

[13] L. Peng, S. Qiao, Z. Xu, F. Guan, Z. Ding, Z. Gu, et al., Effects of culture conditions on monosaccharide composition of Ganoderma lucidum exopolysaccharide and on activities of related enzymes, Carbohydr. Polym. 133 (2015) 104–109, https://doi.org/10.1016/j.carbpol.2015.07.014.

[14] Z. Dong, G. Dong, F. Lai, H. Wu, Q. Zhan, Purification and comparative study of bioactivities of a natural selenized polysaccharide from Ganoderma Lucidum mycelia, Int. J. Biol. Macromol. 190 (2021) 101–112, https://doi.org/10.1016/j.ijbiomac.2021.08.189.

[15] S.A. Heleno, L. Barros, A. Martins, M.J.R.P. Queiroz, C. Santos-Buelga, I.C.F. R. Ferreira, Fruiting body, spores and in vitro produced mycelium of *Ganoderma lucidum* from Northeast Portugal: a comparative study of the antioxidant potential of phenolic and polysaccharidic extracts, Food Res. Int. 46 (2012) 135–140, doi: https://doi.org/10.1016/j.foodres.2011.12.009 extracts, Food Research International 46 (2012) 135–140. doi:https://doi.org/10.1016/j.foodres.2011.12.009.

[16] F. Li, T. Liu, X. Liu, C. Han, L. Li, Q. Zhang, et al., Ganoderma lucidum polysaccharide hydrogel accelerates diabetic wound healing by regulating macrophage polarization, Int. J. Biol. Macromol. 260 (2024) 129682, https://doi.org/10.1016/j.ijbiomac.2024.129682.

[17] R. Sánchez, E. Espinosa, J. Domínguez-Robles, J.M. Loaiza, A. Rodríguez, Isolation and characterization of lignocellulose nanofibers from different wheat straw pulps, Int. J. Biol. Macromol. 92 (2016) 1025–1033, https://doi.org/10.1016/j.ijbiomac.2016.08.019.

[18] R.C. Rudjito, A. Jiménez-Quero, M. Hamzaoui, S. Kohnen, F. Vilaplana, Tuning the molar mass and substitution pattern of complex xylans from corn fibre using subcritical water extraction, Green Chem. 22 (2020) 8337–8352, https://doi.org/10.1039/D0GC02897E.

[19] V.L. Singleton, R. Orthofer, R.M. Lamuela-Raventós, [14] Analysis of total phenols and other oxidation substrates and antioxidants by means of folin-ciocalteu reagent, 1999, pp. 152–178.

[20] C. Menzel, C. González-Martínez, A. Chiralt, F. Vilaplana, Antioxidant starch films containing sunflower hull extracts, Carbohydr. Polym. 214 (2019) 142–151, https://doi.org/10.1016/j.carbpol.2019.03.022.

[21] M. Bradford, A rapid and sensitive method for the quantitation of microgram quantities of protein utilizing the principle of protein-dye binding, Anal. Biochem. 72 (1976) 248–254, https://doi.org/10.1006/abio.1976.9999.

[22] H. Geng, A facile approach to light weight, high porosity cellulose aerogels, Int. J. Biol. Macromol. (118) (2018) 921–931, doi:10.1016/j.ijbiomac.2018.06.167 [22] A. International, ASTM D882-18, Standard Test Method for Tensile Propertes of Thin Plastic Sheetings, (2018).

[23] M. Rostamitabar, A. Ghahramani, G. Seide, S. Jockenhoevel, S. Ghazanfari, Drug loaded cellulose–chitosan aerogel microfibers for wound dressing applications, Cellulose 29 (2022) 6261–6281, https://doi.org/10.1007/s10570-022-04630-6.

[24] P. Thangaraju, S.B. Varthya, ISO 10993: biological evaluation of medical devices, in: Medical Device Guidelines and Regulations Handbook, Springer International Publishing, Cham, 2022, pp. 163–187.

[25] V.G. Wilson, Growth and Differentiation of HaCaT Keratinocytes, 2013, pp. 33–41.

[26] B. Luzak, P. Siarkiewicz, M. Boncler, An evaluation of a new high-sensitivity PrestoBlue assay for measuring cell viability and drug cytotoxicity using EA.hy926 endothelial cells, Toxicol. In Vitro 83 (2022) 105407, https://doi.org/10.1016/j.tiv.2022.105407.

[27] F. Asadi, M. Barshan-tashnizi, A. Hatamian-Zarmi, F. Davoodi-Dehaghani, B. Ebrahimi-Hosseinzadeh, Enhancement of exopolysaccharide production from Ganoderma lucidum using a novel submerged volatile co-culture system, Fungal Biol. 125 (2021) 25–31, https://doi.org/10.1016/j.funbio.2020.09.010.

[28] J.Y. Kang, B. Lee, C.H. Kim, J.H. Choi, M.-S. Kim, Enhancing the prebiotic and antioxidant effects of exopolysaccharides derived from Cordyceps militaris by enzyme-digestion, LWT 167 (2022) 113830, https://doi.org/10.1016/j.lwt.2022.113830.

[29] Q. Dong, D. He, X. Ni, H. Zhou, H. Yang, Comparative study on phenolic compounds, triterpenoids, and antioxidant activity of Ganoderma lucidum affected by different drying methods, J. Food Meas. Charact. 13 (2019) 3198–3205, https://doi.org/10.1007/s11694-019-00242-0.

[30] M. Hamidi, O.V. Okoro, K. Rashidi, M.S. Salami, R. Mirzaei Seveiri, H. Samadian, et al., Evaluation of two fungal exopolysaccharides as potential biomaterials for wound healing applications, World J. Microbiol. Biotechnol. 39 (2023) 49, https://doi.org/10.1007/s11274-022-03459-2.

[31] T. Lu, Q. Li, W. Chen, H. Yu, Composite aerogels based on dialdehyde nanocellulose and collagen for potential applications as wound dressing and tissue engineering scaffold, Compos. Sci. Technol. 94 (2014) 132–138, https://doi.org/10.1016/j.compscitech.2014.01.020 [32] Parajuli, P., Acharya, S., Shamshina, J. L., Abidi, N. Tuning the morphological properties of cellulose aerogels: an investigation of salt-mediated preparation. Cellulose. 2021; 28: 7559. doi:10.1007/s10570-021-04028-w.

[32] X. Liu, Y. Niu, K.C. Chen, S. Chen, Rapid hemostatic and mild polyurethane-urea foam wound dressing for promoting wound healing, Mater. Sci. Eng. C 71 (2017) 289, https://doi.org/10.1016/j.msec.2016.10.019.

[33] A.D. French, Idealized powder diffraction patterns for cellulose polymorphs, Cellulose 21 (2014) 885, https://doi.org/10.1007/s10570-013-0030-4.

[34] N. Siti Syazwani, M.N. Ervina Efzan, C.K. Kok, M.J. Nurhidayatullaili, Analysis on extracted jute cellulose nanofibers by Fourier transform infrared and X-ray diffraction, J. Build. Eng. 48 (2022) 103744, https://doi.org/10.1016/j.jobe.2021.103744.

[35] R. Morcillo-Martín, E. Espinosa, L. Rabasco-Vílchez, L.M. Sanchez, J. de Haro, A. Rodríguez, Cellulose nanofiber-based aerogels from wheat straw: influence of surface load and lignin content on their properties and dye removal capacity, Biomolecules 12 (2022) 232, https://doi.org/10.3390/biom12020232.

[36] M. Zhang, N. Guo, Y. Sun, J. Shao, Q. Liu, X. Zhuang, et al., Nanocellulose aerogels from banana pseudo-stem as a wound dressing, Ind. Crop Prod. 194 (2023) 116383, https://doi.org/10.1016/j.indcrop.2023.116383.

[37] F. Cahn, T.R. Kyriakides, Generation of an artificial skin construct containing a non-degradable fiber mesh: a potential transcutaneous interface, Biomed. Mater. 3 (2008) 034110, https://doi.org/10.1088/1748-6041/3/3/034110.

[38] Y.I. Heit, P. Dastouri, D.L. Helm, G. Pietramaggiori, G. Younan, P. Erba, et al., Foam pore size is a critical interface parameter of suction-based wound healing devices, Plast. Reconstr. Surg. 129 (2012) 589–597, https://doi.org/10.1097/PRS.0b013e3182402c89.

[39] I.V. Yannas, E. Lee, D.P. Orgill, E.M. Skrabut, G.F. Murphy, Synthesis and characterization of a model extracellular matrix that induces partial regeneration of adult mammalian skin, Proc. Natl. Acad. Sci. 86 (1989) 933–937, https://doi.org/10.1073/pnas.86.3.933.

[40] S.M. Lee, I.K. Park, Y.S. Kim, H.J. Kim, H. Moon, S. Mueller, et al., Physical, morphological, and wound healing properties of a polyurethane foam-film dressing, Biomater. Res. 20 (2016) 15, https://doi.org/10.1186/s40824-016-0063-5.

[41] A. Gefen, P. Alves, D. Beeckman, J.L. Lázaro-Martínez, H. Lev-Tov, B. Najafi, et al., Mechanical and contact characteristics of foam materials within wound dressings: theoretical and practical considerations in treatment, Int. Wound J. 20 (2023) 1960–1978, https://doi.org/10.1111/iwj.14056.

[42] N. Faucher, H. Safar, M. Baret, A. Philippe, R. Farid, Superabsorbent dressings for copiously exuding wounds, Br. J. Nurs. 21 (2012) S22, https://doi.org/10.12968/bjon.2012.21.Sup12.S22.

[43] G. Singh, C. Byrne, H. Thomason, A.J. McBain, Investigating the microbial and metalloprotease sequestration properties of superabsorbent wound dressings, Sci. Rep. 12 (2022) 4747, https://doi.org/10.1038/s41598-022-08361-3.

[44] R. Khan, M.U. Aslam Khan, G.M. Stojanović, A. Javed, S. Haider, S.I. Abd Razak, Fabrication of bilayer nanofibrous-hydrogel scaffold from bacterial cellulose, PVA, and gelatin as advanced dressing for wound healing and soft tissue engineering, ACS Omega 9 (2024) 6527, https://doi.org/10.1021/acsomega.3c06613.

[45] M. Rottmar, M. Richter, X. Mäder, K. Grieder, K. Nuss, A. Karol, B. von Rechenberg, E. Zimmermann, S. Buser, A. Dobmann, J. Blume, A. Bruinink, In vitro investigations of a novel wound dressing concept based on biodegradable

polyurethane, Sci. Technol. Adv. Mater. 16 (2015) 034606, https://doi.org/10.1088/1468-6996/16/3/034606.
[46] Y. Feng, X. Li, Q. Zhang, S. Yan, Y. Guo, M. Li, R. You, Mechanically robust and flexible silk protein/polysaccharide composite sponges for wound dressing, Carbohydr. Polym. 216 (2019) 17, https://doi.org/10.1016/j.carbpol.2019.04.008.
[47] M.C. Li, Q. Wu, K. Song, H.N. Cheng, S. Suzuki, T. Lei, Chitin nanofibers as reinforcing and antimicrobial agents in carboxymethyl cellulose films: influence of partial deacetylation, ACS Sustain. Chem. Eng. 4 (2016) 4385, https://doi.org/10.1021/acssuschemeng.6b00981.
[48] S. De Carolis, C. Putignano, L. Soria, G. Carbone, Effect of porosity and pore size distribution on elastic modulus of foams, Int. J. Mech. Sci. 261 (2024) 108661, https://doi.org/10.1016/j.ijmecsci.2023.108661.
[49] C. Torres-Sanchez, F.R.A. Al Mushref, M. Norrito, K. Yendall, Y. Liu, P.P. Conway, The effect of pore size and porosity on mechanical properties and biological response of porous titanium scaffolds, Mater. Sci. Eng. C 77 (2017) 219, https://doi.org/10.1016/j.msec.2017.03.249.
[50] L. Tang, Z. Guo, Q. Zhao, X. Fan, Y. Pu, B. He, J. Chen, A biodegradable Janus sponge for negative pressure wound therapy, Biomacromolecules 25 (2024) 2542, https://doi.org/10.1021/acs.biomac.4c00046.
[51] R. Portela, C.R. Leal, P.L. Almeida, R.G. Sobral, Bacterial cellulose: a versatile biopolymer for wound dressing applications, J. Microbial. Biotechnol. 12 (2019) 586–610, https://doi.org/10.1111/1751-7915.13392.
[52] J.-Y. Liu, Y. Li, Y. Hu, G. Cheng, E. Ye, C. Shen, et al., Hemostatic porous sponges of cross-linked hyaluronic acid/cationized dextran by one self-foaming process, Mater. Sci. Eng. C 83 (2018) 160–168, https://doi.org/10.1016/j.msec.2017.10.007.
[53] M.F. Elahi, G. Guan, L. Wang, M.W. King, Improved hemocompatibility of silk fibroin fabric using layer-by-layer polyelectrolyte deposition and heparin immobilization, J. Appl. Polym. Sci. 131 (2014), https://doi.org/10.1002/app.40772.
[54] ASTM International, ASTM F756-17 Standard Practice for Assesment of Hemolytic Properties of Materials. https://www.astm.org/f0756-17.html, 2017.
[55] P.A. Zaitun Hasibuan, Yuandani, M. Tanjung, S. Gea, K.M. Pasaribu, M. Harahap, et al., Antimicrobial and antihemolytic properties of a CNF/AgNP-chitosan film: a potential wound dressing material, Heliyon 7 (2021) e08197, https://doi.org/10.1016/j.heliyon.2021.e08197.
[56] M. Kempf, R.M. Kimble, L. Cuttle, Cytotoxicity testing of burn wound dressings, ointments and creams: a method using polycarbonate cell culture inserts on a cell culture system, Burns 37 (2011) 994–1000, https://doi.org/10.1016/j.burns.2011.03.017.
[57] B. Boonkaew, M. Kempf, R. Kimble, L. Cuttle, Cytotoxicity testing of silver-containing burn treatments using primary and immortal skin cells, Burns 40 (2014) 1562–1569, https://doi.org/10.1016/j.burns.2014.02.009.
[58] C. Yadav, M. Chhajed, P. Choudhury, R.P. Sahu, A. Patel, S. Chawla, et al., Bio-extract amalgamated sodium alginate-cellulose nanofibres based 3D-sponges with interpenetrating BioPU coating as potential wound care scaffolds, Mater. Sci. Eng. C 118 (2021) 111348, https://doi.org/10.1016/j.msec.2020.111348.
[59] O. Simonetti, S. Marasca, M. Candelora, G. Rizzetto, G. Radi, E. Molinelli, L. Brescini, O. Cirioni, A. Offidani, Methicillin-resistant Staphylococcus aureus as a cause of chronic wound infections: alternative strategies for management, AIMS Microbiol. 8 (2) (2022) 125–137, https://doi.org/10.3934/microbiol.2022011.
[60] J. Chen, L. Zhao, J. Ling, L.-Y. Yang, X. Ouyang, A quaternized chitosan and carboxylated cellulose nanofiber-based sponge with a microchannel structure for rapid hemostasis and wound healing, Int. J. Biol. Macromol. 233 (2023) 123631, https://doi.org/10.1016/j.ijbiomac.2023.123631.
[61] M. Zhou, J. Liao, G. Li, Z. Yu, D. Xie, H. Zhou, et al., Expandable carboxymethyl chitosan/cellulose nanofiber composite sponge for traumatic hemostasis, Carbohydr. Polym. 294 (2022) 119805, https://doi.org/10.1016/j.carbpol.2022.119805.
[62] L. Wang, C. Zhang, W. Zhao, W. Li, G. Wang, X. Zhou, et al., Water-swellable cellulose nanofiber aerogel for control of hemorrhage from penetrating wounds, ACS Appl. Bio Mater. 5 (2022) 4886–4895, https://doi.org/10.1021/acsabm.2c00609.
[63] X. Fan, Y. Li, X. Li, Y. Wu, K. Tang, J. Liu, et al., Injectable antibacterial cellulose nanofiber/chitosan aerogel with rapid shape recovery for noncompressible hemorrhage, Int. J. Biol. Macromol. 154 (2020) 1185–1193, https://doi.org/10.1016/j.ijbiomac.2019.10.273.
[64] L. Liu, L. Liu, L. Chen, G. Chen, Y. Wei, F.F. Hong, Synthesis of hemostatic aerogel of TEMPO-oxidized cellulose nanofibers/collagen/chitosan and in vivo/vitro evaluation, Mater. Today Bio 28 (2024) 101204, https://doi.org/10.1016/j.mtbio.2024.101204.
[65] C. Yadav, A. Saini, K. Li, S. Chawla, X. Li, W.-D. Jang, Cinnamomum cassia perfused nanocellulose-based biocompatible sponge for hemostatic wound care dressing, Cellulose 30 (2023) 5857–5870, https://doi.org/10.1007/s10570-023-05252-2.